Marine Pollution Bulletin 119 (2017) 336–350

Contents lists available at ScienceDirect

Marine Pollution Bulletin

journal homepage: www.elsevier.com/locate/marpolbul

Operational oil spill trajectory modelling using HF radar currents: A northwest European continental shelf case study

Ana J. Abascal[a,*], Jorge Sanchez[b], Helios Chiri[a], María I. Ferrer[b], Mar Cárdenas[a], Alejandro Gallego[c], Sonia Castanedo[d], Raúl Medina[a], Andrés Alonso-Martirena[b], Barbara Berx[c], William R. Turrell[c], Sarah L. Hughes[c]

[a] Environmental Hydraulics Institute, Universidad de Cantabria, Avda. Isabel Torres, 15, Parque Científico y Tecnológico de Cantabria, 39011 Santander, Spain
[b] Qualitas Remos, Madrid, Spain
[c] Marine Scotland Science, Marine Laboratory, Aberdeen, Scotland, United Kingdom
[d] Departamento de Ciencias y Técnicas del Agua y del Medio Ambiente, E.T.S.I. de Caminos Canales y Puertos, Universidad de Cantabria, Avda. de los Castros s/n, 39005 Santander, Spain

ARTICLE INFO

Keywords:
HF radar
Operational forecasting
Oil spill modelling
Drifting buoys

ABSTRACT

This paper presents a novel operational oil spill modelling system based on HF radar currents, implemented in a northwest European shelf sea. The system integrates Open Modal Analysis (OMA), Short Term Prediction algorithms (STPS) and an oil spill model to simulate oil spill trajectories. A set of 18 buoys was used to assess the accuracy of the system for trajectory forecast and to evaluate the benefits of HF radar data compared to the use of currents from a hydrodynamic model (HDM). The results showed that simulated trajectories using OMA currents were more accurate than those obtained using a HDM. After 48 h the mean error was reduced by 40%. The forecast skill of the STPS method was valid up to 6 h ahead. The analysis performed shows the benefits of HF radar data for operational oil spill modelling, which could be easily implemented in other regions with HF radar coverage.

1. Introduction

Oil spill pollution and its impact on coastal and marine environments have led to a growing concern regarding oil spill preparedness and response. Over the last decade, many operational oceanographic systems that are based on oil spill numerical models coupled to hydrodynamic and meteorological models have been set up in order to provide decision makers with oil spill trajectory forecasting. Recent oil spill incidents, such as the *Prestige* incident in Spain (2002) and the *Deepwater Horizon* oil spill in the Gulf of Mexico (2010), have demonstrated that forecasting oil spill trajectory is fundamental for planning and mitigation strategies (Castanedo et al., 2006; Liu et al., 2011a, b, c). Besides forecast applications, Lagrangian trajectory models have been used and incorporated into operational systems which are run backwards in time, with the purpose of detecting likely release sites, illegal discharges and potential polluters (Ambjörn, 2008; Christiansen, 2003; Abascal et al., 2012).

The accuracy of the simulations provided by these oil spill simulation systems is highly dependent on the accuracy of the met-ocean forcing data used to force the oil spill model. These forcing data are usually provided by hydrodynamic and atmospheric models, which have associated uncertainty which may affect the accuracy of the oil spill forecast and backtracking simulation (Edwards et al., 2006; Price et al., 2006). Such uncertainty becomes greater in ocean circulation modelling of coastal areas, where the complex patterns that characterize coastal hydrodynamics complicate the forecasting of the current field. High frequency (HF) radar systems become an alternative for the provision of accurate surface current maps in near coastal environments. HF Radar is nowadays the only technology capable of providing real time surface currents continuous in space and time for wide areas, from a few kilometers to up to 200 km offshore. In the last few years, several studies have been carried out to validate this technology (e.g. Graber et al., 1997; Kaplan et al., 2005; Hubbard et al., 2013; Lorente et al., 2014) and to assess the effectiveness of using HF radar currents for trajectory analysis (e.g. Ullman et al., 2003; O'Donnell et al., 2005; Ullman et al., 2006; Abascal et al., 2012; Liu et al., 2014).

Recent experiments, such as the NOAA sponsored Safe Seas 2006 exercise (Long and Barrick, 2007) and the Galicia HF Radar Experience (Abascal et al., 2009), have shown the benefits that HF radar currents can provide for the tracking and simulation of oil spills. However, a

* Corresponding author.
E-mail address: abascalaj@unican.es (A.J. Abascal).

http://dx.doi.org/10.1016/j.marpolbul.2017.04.010
Received 25 November 2016; Received in revised form 23 March 2017; Accepted 3 April 2017
Available online 23 April 2017

possible limitation to the use of HF radar for this purpose arises from the data gaps that HF radar, as any other remote sensing system, is subject to. Data gaps are predominately due to environmental effects, such as increased external noise or low signal due to ocean surface conditions. Many applications of HF radar surface current data require these gaps to be filled, such as Lagrangian numerical models used to estimate material transport and dispersion. Several studies have proposed different methodologies to accurately reconstruct hourly HF radar surface current data to provide gap-free current fields, e.g. Open-Boundary Modal Analysis (OMA) (Lekien and Gildor, 2009; Barrick et al., 2012; Roarty et al., 2016).

In order to increase the benefits of this technology for search and rescue, safety in navigation, and oil spill modelling, and to improve trajectory forecasts during emergency-response situations, recent studies have successfully provided accurate short term current forecasts based on assimilation of HF radar currents into coastal ocean models (Breivik and Sætra, 2001; Oke et al., 2002; Paduan and Shulman, 2004; Hoteit et al., 2009). Efforts have also been made to use longer time series of HF radar surface current maps to make short-term forecasts (Zelenke, 2005; Frolov et al., 2011). Whereas these forecast methods using HF radar data employed methodologies that relied on a month or more of historic data to forecast tides and background residual circulation, this will not be possible in the scenario of a rapid deployment of an HF radar system to a new area in an oil spill emergency situation. To overcome this limitation, Barrick et al. (2012) designed and validated a real-time gap-filling technique for HF radar data and a short-term prediction system (STPS) methodology that relied only on 12 h of HF radar currents from a system deployed in Norway.

Despite its potential, developments that make use of the information provided by HF radar technology, translating it into added value products to support decision making in oil spill response or oil and gas platform operation, are currently scarce. While HF radar systems have been mainly used for search and rescue emergencies (Barrick et al., 2012; Breivik et al., 2013), there is a lack of operational applications for oil spills, especially in Europe.

To study the benefits which an HF radar system could bring to the UK coast, the Brahan Project (http://www.thebrahanproject.com/) was carried out in northern Scotland as a joint effort between several public institutions and oil and gas companies (Turrell et al., 2014). The main goal of this project was to provide a fully operational Long Range SeaSonde HF radar system in the Shetland-Orkney area (Fig. 1) to measure surface currents in near real time.

Within the framework of the project “NEw MetOcean Tools for the Oil and Gas Industry” (http://www.nemot4ogi.com), an oil spill forecasting and backtracking system was implemented in the Brahan study area to show the capabilities of HF radar systems for oil spill preparedness and response. The system integrates Open Modal Analysis (OMA), Short Term Predicted algorithms (STPS) and an oil spill numerical model to simulate oil spills in real time into a web-based information system. The oil spill forecasting capability of the system was extensively validated by means of a set of 18 drifting buoys released in the study area. A sensitivity analysis was carried out to assess the accuracy of OMA and STPS velocity fields for oil spill simulations and to evaluate the benefits of HF radar data compared to the use of HDM currents.

2. Study area

The Orkney Islands are situated directly north of the Scottish mainland, separated by the ca. 10 km wide Pentland Firth. The Shetland Islands are to the north west of Orkney, separated by a channel approximately 80 km wide, the Fair Isle Gap (FIG), named after the small island (Fair Isle) in the middle. Water depths around and between Orkney and Shetland (collectively known as the Northern Isles) are generally < 100 m, compared to slightly deeper waters in the northern North Sea to the east and the continental shelf to the west. The island chain made up by Orkney and Shetland, and the relatively shallower ridge of the FIG create a natural physical border which, to some extent, presents a barrier to the exchange of water with the North Atlantic (Turrell, 1992a; Huthnance, 1997). However, this is an important area of water inflow into the northern North Sea. Waters enter the North Sea from the North Atlantic through the northern open boundary via three main routes (Otto et al., 1990; Svendsen et al., 1991; Turrell, 1992b): through the FIG, around the north and east of the Shetland Islands (the East Shetland Atlantic Inflow, ESAI) and along the western side of the Norwegian Trench (Norwegian Trench inflow). The northern North Sea ecosystem variability (including regime shifts) has been linked to changes in the Atlantic inflow (e.g. Beaugrand, 2004). The Brahan HF Radar system covered the FIG and adjacent waters to the east and west; the radar sites were located at North Ronaldsay (Orkney) and Sumburgh (Shetland), with coverage with an average range of > 100 km (see below). The FIG is an important maritime transport corridor, including for oil tankers (the MV *Braer* ran aground on the southern tip of Shetland in 1993, spilling 85,000 t of Norwegian Gullfaks crude oil) and the waters around the Northern Isles are subject to a wide range of important socio-economic activities such as shipping, tourism, aquaculture, fishing and oil and gas extraction.

3. Description of the operational system

The main goal of our operational system is to provide short term (12–48 h) oil spill trajectory forecasting and backtracking. The system is comprised of three components: 1) Met-ocean Data Module that provides hourly surface currents with ~ 4 km spatial resolution and gap-free HF radar surface currents based on Open Modal Analysis. This module also integrates wind forecast from the Global Forecast System (GFS) model (NOAA) (Environmental Modeling Center, 2003); 2) Numerical Module that includes: i) a Short Term Prediction System that provides 12 h forecast currents using HF radar measurements and ii) an oil spill transport and fate model, TESEO (Abascal et al., 2007); and 3) Web-based Information System that is able to provide all relevant information, in an operational way to the end user, which is needed to support decision making for the purposes of oil spill response.

In the case of an oil spill, the system allows the user: 1) to forecast the transport and fate of the spill with a forecast horizon of 12 h, using GFS wind and STPS surface currents and 2) to perform trajectory backtracking with a simulation horizon of 48 h, using OMA surface currents and GFS winds.

A general overview of the system is displayed in Fig. 2 and its description is presented below.

3.1. Met-ocean data module

3.1.1. HF radar currents

The HF radar technology works on the principle of Bragg scattering where the transmitted electromagnetic radio waves are reflected by resonant ocean surface waves with half of the incident radar wavelength (Barrick et al., 1977). An HF radar system consists of a transmitter antenna transmitting high-frequency (3–50 MHz) electromagnetic waves over a conductive ocean surface and receiver antennas capturing the backscattered signal with a Doppler frequency shift resulting from the moving ocean surface due to waves and underlying (surface) currents. The main data product is 2-D surface current maps, which require two or more radars with overlapping coverage (Barrick et al., 1977; Lipa and Barrick, 1986). HF coastal radars have evolved over the past 40 years into worldwide operational networks that provide real time data to a variety of end users (Harlan et al., 2010).

HF radar surface currents used by the Operational Oil Spill Modelling System were provided by two CODAR HF radar stations that were installed in Northern Scotland as part of the Brahan project: one at Sumburgh lighthouse (Shetland), and one at North Ronaldsay light-

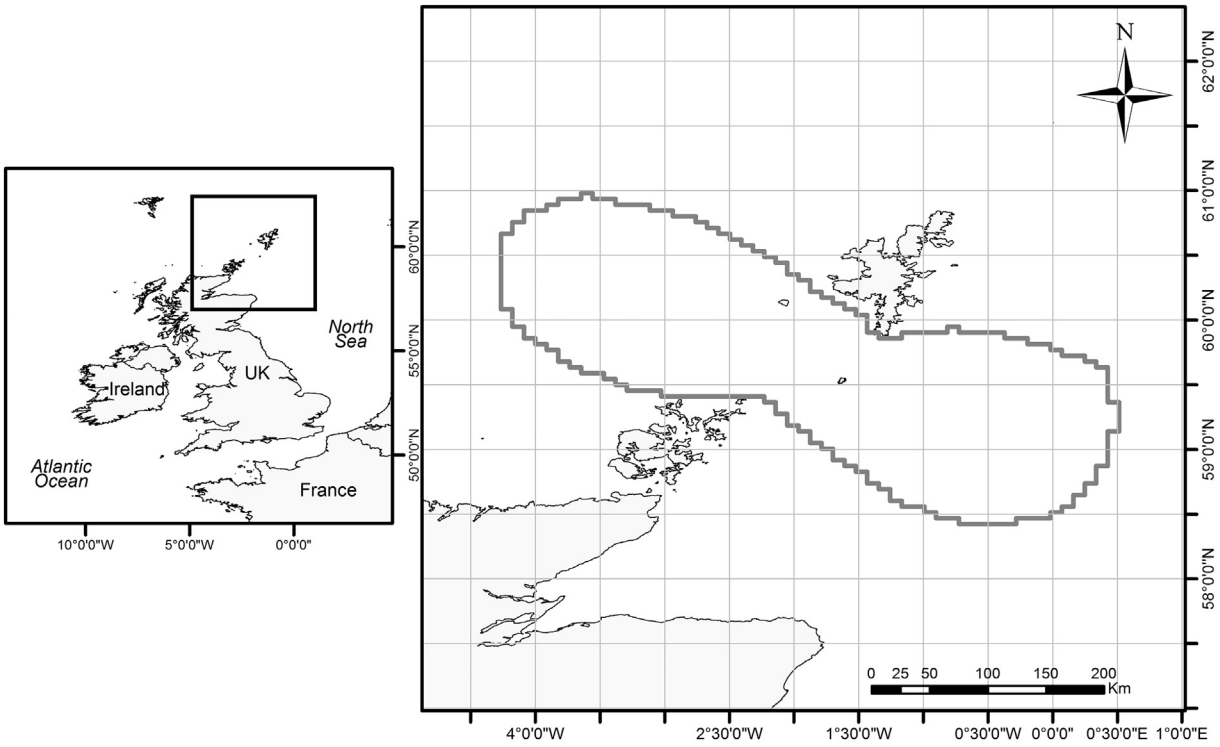

Fig. 1. Study area and HF radar system domain (grey line in right panel).

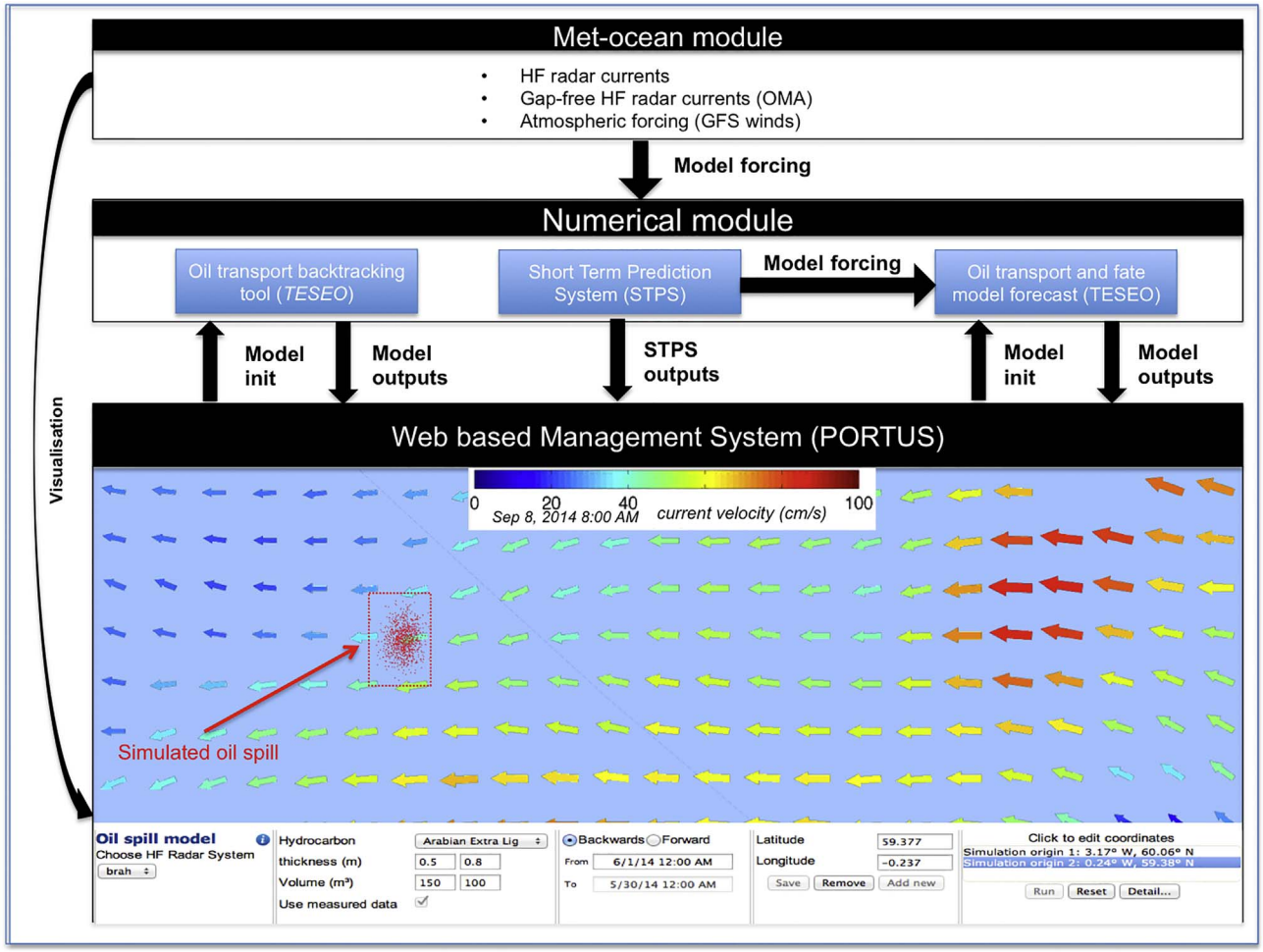

Fig. 2. Flowchart of the operational system.

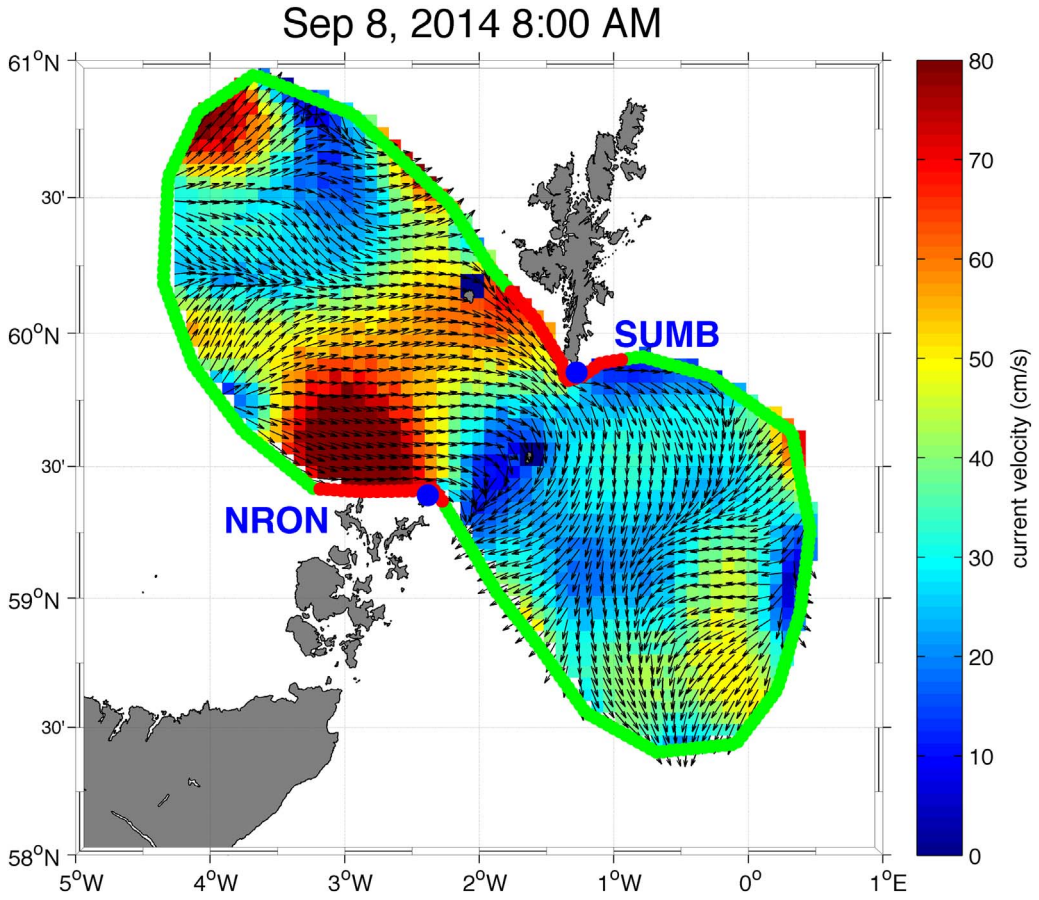

Fig. 3. Example of total OMA surface currents map in the Brahan area and OMA domain. OMA closed boundaries (red line) and open boundaries (green line) are also shown. (For interpretation of the references to colour in this figure legend, the reader is referred to the web version of this article.)

house (Orkney). Both stations operated at a central frequency of 4.5 MHz with a bandwidth of 36.8 kHz and a sweep rate of 1 Hz. With these specifications, each radar measured radial components of the surface current with an average range of 110 km, range resolution of 4 km and azimuth accuracy of 5°. A first study of currents, waves, wind direction and their interplay in this interesting area based on Brahan HF radar currents can be found in Lipa et al. (2014).

The radial vector files generated by the two CODAR systems at 1 h intervals were combined to generate the total vector field with respect to a predefined surface grid of 5 × 5 km horizontal resolution using the OMA method (Kaplan and Leiken, 2007), as described in more detail in the next section of this paper. A typical total vector plot for this system is shown in Fig. 3. It is important to note here that, due to the technical characteristics of the radar system, the effective depth of measurements is of the order of 2 m (Stewart and Joy, 1974). The data collection started on the 1st September 2013 and stopped at the end of August 2014, when the radars were decommissioned. The oil spill trajectory system described in this paper worked operationally between June 2014 and August 2014.

3.1.2. OMA currents

Surface currents used by the Oil Spill Modelling System need to be spatially and temporally homogenous. However, spatial gaps can occur in the HF radar surface currents fields due to geometric instabilities along the baseline between radar sites, shadowing from local coastline geometry, ship echoes, radio frequency interferences, or antenna interaction with the near-field environment. For this reason, a gap-filling technique based on OMA has been applied to the radial currents fields provided by each of the two Brahan HF radar stations. It becomes an important component of coastal ocean observing systems (Liu et al., 2015).

The OMA method (Kaplan and Leiken, 2007) is based on representing the flow near the surface in terms of a divergence-free stream function ψ, vorticity free velocity potential φ and a boundary function with a portion of the boundary "closed" and the remainder as an open boundary (φ^b), defined depending on the domain.

These scalar fields ψ, φ and φ^b are the eigenfunction solutions for the three Laplace equations

$$\nabla^2\Psi_i + \lambda_i^{\Psi}\Psi_i = 0;\ \nabla^2\phi_i + \lambda_i^{\phi}\phi_i = 0;\ \nabla^2\phi_i^b + \lambda_i^b\phi_i^b = 0 \tag{1}$$

These eigenfunctions (ψ_i, φ_i, and φ_i^b) are called OMA modes. These modes need to be calculated only once using finite element methods for a given radar geometry, being then stored.

Surface current is calculated as a linear combination of the OMA modes where the coefficients (α_i^{ψ}, α_i^{φ}, α_i^b) are fitted using linear least-squares (LS) to the radar-observed current fields.

$$\vec{u}(x,y,t) = \sum_{i=1}^{\infty} a_i^{\Psi}(t)\nabla\times\Psi_i(x,y)\hat{k} + \sum_{i=1}^{\infty} a_i^{\varphi}(t)\nabla\varphi_i(x,y) + \sum_{i=0}^{\infty} a_i^b(t)\nabla\varphi_i^b(x,y) \tag{2}$$

The OMA coefficients ($\alpha_i^{\psi}(t)$,$\alpha_i^{\varphi}(t)$ and $\alpha_i^b(t)$) are used to perform the short-term prediction. The prediction is based on an adjustment of these coefficients into a temporal model of 12 h and extrapolation is used to reconstruct velocity fields for the next 12 h using Eq. (2). A more detailed explanation will be given in the following section.

For the Brahan region of interest, the OMA modes were calculated in the defined domain shown in Fig. 3 where the closed boundaries (red line) and open boundaries (green line) are also shown. Fig. 4 shows the first OMA modes (sorted by the eigenvalues in Eq. (1)) for non-

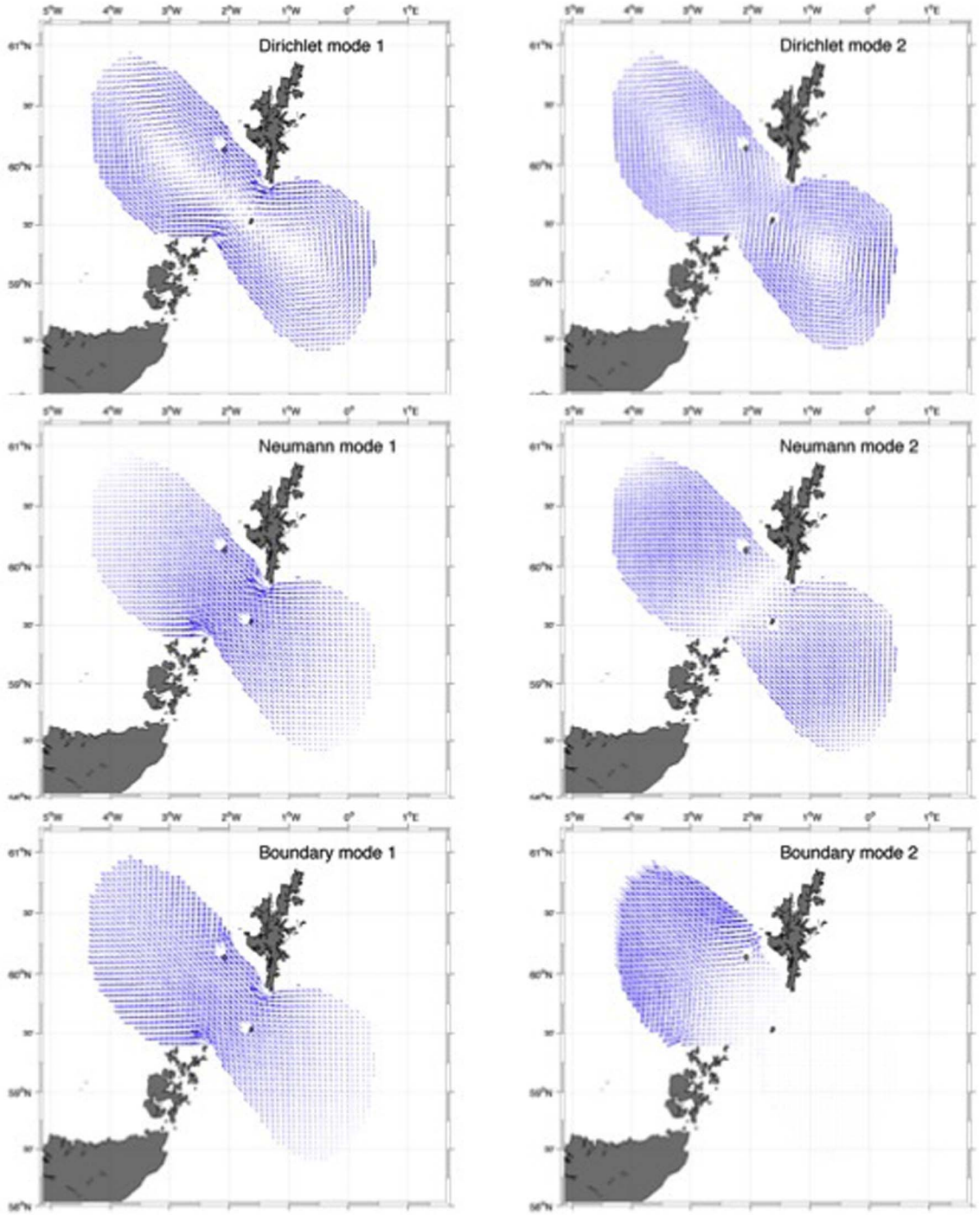

Fig. 4. OMA modes. Upper panels for Dirichlet (vorticity), middle panels for Neumann (divergence) and lower panels for Boundary.

divergent modes (Dirichlet), non-rotational modes (Neumann) and Boundary modes (flow in and out the domain). Lower-order modes represent larger circulation scales while higher-order modes represent smaller scales. The number of modes used is defined by the minimum scale resolution of the modes; in our case it is fixed to 40 km. This gives, according to Eq. (1), 11 Dirichlet modes, 22 Neumann modes and 18 Boundary modes.

Rigorous justification for the OMA mathematics summarized above can be found in Lipphardt et al. (2000) and Lekien and Coulliette (2004). Further description and validation of OMA for CODAR HF radar current measurements can be found in Barrick et al. (2012).

3.1.3. Atmospheric data

The atmospheric forcing fields were obtained from the NOAA National Center for Environmental Prediction (Environmental Modeling Center, 2003). This system provides a 5-day wind forecast with 0.5° spatial and 3-hourly temporal resolution. These data are served by NOAA Operational Model Archive and Distribution System (NOMADS) (Rutledge et al., 2006) using the GrADS-DODS/OPeNDAP Server (GDS).

3.2. Numerical module

3.2.1. STPS currents

The methodology introduced in Barrick et al. (2012) has been used

to develop a Short Time Prediction System (STPS) for surface currents in the Brahan radar coverage area, based on a very short time history of HF radar currents, using OMA-fitted surface current coefficients.

In order to implement this prediction method, the OMA coefficients corresponding to all three sets of modes (Dirichlet, Neumann and Boundary) are selected, based on the data from the last 12 h immediately before the current prediction time. Thus, for each prediction time there is a coefficient vector $A_j^{(i)}$ representing the OMA coefficients: $[a_i^{\Psi}(t_j), a_i^{\varphi}(t_j), a_i^{b}(t_j)]$.

Each of these OMA coefficients for the 12 h immediately before the prediction time can then be fitted to a sequence with different terms: a constant, a linear trend and a cosine and sine series with different temporal frequencies such as the inertial frequency and the most important tidal constituents in the area where the prediction methodology is to be applied. The inertial frequency is calculated as $f_0 2\Omega \sin(\vartheta)$, where ϑ is the latitude of the radar area and Ω is the earth angular rotation rate in radians s^{-1}. In our case, the latitude at the midpoint between northernmost and southernmost edges of the OMA domain was used. In our area of interest in northern Scotland, the most important tidal constituent is the semidiurnal M2 ($f_1 = \frac{1}{12{,}42}\ hours^{-1}$).

Then, each of the temporal modes can be written as follows.

$$A_j^{(i)} = B_1^{(i)} + B_2^{(i)} t_j + B_3^{(i)} cos(f_1 t_j) + B_4^{(i)} sin(f_1 t_j) + B_5^{(i)} cos(f_0 t_j) + B_6^{(i)} sin(f_0 t_j) \quad (3)$$

The STPS temporal modal coefficients $B_n^{(i)}$ are considered to be unknown for each of the i OMA modes. These relations can be expressed more compactly in matrix form as:

$$[A_j^{(i)}] = [M_{j,n}][B_n^{(i)}] \quad (4)$$

With the model matrix represented in Eq. (4) above determined at each of the time points from the known OMA coefficients $A_j^{(i)}$, the overdetermined system of equations is solved using any standard approach. In this case MATLAB has been used where the solution is denoted by the backslash operator as follows:

$$[B_n^{(i)}] = [M_{j,n}] \backslash [A_j^{(i)}] \quad (5)$$

The coefficients for the N temporal modes, $B_n^{(i)}$, that are determined by Eq. 5 allow forecasts ahead to be made by constructing new model matrices for future times k and performing a forward matrix multiplication:

$$[A_{j+k}^{(i)}] = [M_{j+k,n}][B_n^{(i)}] \quad (6)$$

Then, from these new "forecasted" OMA coefficients as a function of time, the total vector fields at future times t_{J+k} (k = 1,12) are created.

As a measure of forecast skill for the STPS technique, trajectories of multiple virtual particles in the HF radar domain area forced by the STPS-derived currents are computed and results are compared with actual trajectories of real drifters released in the area by Marine Scotland Science (MSS) during two different exercises in October and December 2013 (see Section 4).

3.2.2. Oil spill numerical model

The oil spill numerical model is based on the TESEO model developed by the Environmental Hydraulics Institute of the University of Cantabria (IHCantabria) (Abascal et al., 2007). The numerical model consists of a transport and a weathering module to represent the evolution of oil spilled in the marine environment. The transport module derives from the two-dimensional Lagrangian model developed by the University of Cantabria as part of the operational forecasting system built to respond to the *Prestige* oil spill (Castanedo et al., 2006). In this model, the drift process of the spilled oil is described by tracking independent numerical particles equivalent to the oil slick. The evolution of the horizontal position of each particle is defined by a combined effect of advective and diffusive velocities:

$$\frac{d\vec{x_i}}{dt} = \vec{u_a}(\vec{x_i}, t) + \vec{u_d}(\vec{x_i}, t) \quad (7)$$

where $\vec{u_a}(\vec{x_i}, t)$is the advective velocity at *i-th* particle position at time step t and $\vec{u_d}(\vec{x_i}, t)$ is the diffusive velocity at the same point and the same time. The model has two options to solve the Lagrangian equation: an explicit Euler scheme and a 4th order Runge-Kutta method. In this study, the Euler option was selected to calculate the oil trajectories. Advective velocity $\vec{u_a}$ is calculated as the linear combination of current and wind velocity and wave-induced Stokes drift, expressed as

$$\vec{u_a} = \vec{u_c} + C_D \vec{u_W} + C_H \vec{u_H} \quad (8)$$

where $\vec{u_C}$ is the surface current velocity; $\vec{u_W}$ is the wind velocity at a height of 10 m over the sea surface; $\vec{u_H}$ is the wave-induced Stokes drift, calculated as $\vec{u_H} = (gH)/8c$, where g is the gravitational acceleration, H is the wave height and c is the wave celerity (Dean and Dalrymple, 1991), calculated as $c = L/T$as a function of wave length ($L = \frac{gT^2}{2\pi}$) and wave period. C_D is the wind drag coefficient and C_H is the wave coefficient. C_D, varies from 2.5% to 4.4% of the wind speed, with a mean value of 3–3.5% (ASCE, 1996). Given the spatial scale of application of the model in this work, the Stoke's drift has been discarded with respect to the effect of winds and currents on the oil spill transport.

The turbulent diffusive velocity is obtained using a Monte Carlo sampling in the range of velocities $[-\vec{u_d}, \vec{u_d}]$ that are assumed proportional to the diffusion coefficients (Maier-Reimer and Sündermann, 1982; Hunter et al., 1993). The velocity fluctuation for each time step, Δt, is defined as

$$|\vec{u_d}| = \sqrt{\frac{6D}{\Delta t}} \quad (9)$$

where D is the diffusion coefficient, typically in the range of 1–100 $m^2\ s^{-1}$ (ASCE, 1996). Note that for backtracking purposes, the turbulent diffusive velocity is set to zero.

The weathering module includes the process of slick spreading under gravity and viscous forces (Fay, 1971), the evaporation from the slick of the lighter components of the spilled oil (Stiver and MacKay, 1984), the entrainment of water into the oil slick forming emulsions (MacKay et al., 1980) and the change of physicochemical properties. Both components of the model, the transport and the weathering module, have been validated in previous studies (Abascal et al., 2007, 2009; Castanedo et al., 2014).

This paper focuses on the analysis and validation of the oil spill trajectory forecasting capability only and does not make use of the backtracking and weathering modules of the system.

3.3. Web-based information system

A user-friendly web based information system has been developed in order to integrate and manage the described operational system. This information system is based on the PORTUS Marine Information System (http://www.qualitasremos.com/?page_id=1103) developed by QUALITAS.

This information and management system provides:

- Access to, and visual display of, all available met-ocean data (HF radar surface currents fields, atmospheric data, STPS and OMA surface currents fields…).
- The capability to set up, run and display oil spill trajectory simulations (forecast and backtracking) using the TESEO oil spill transport and fate model.
- The capability to export all system outputs in different formats (KMZ, ASCII, NetCDF) through different protocols (ftp and OPeNDAP)

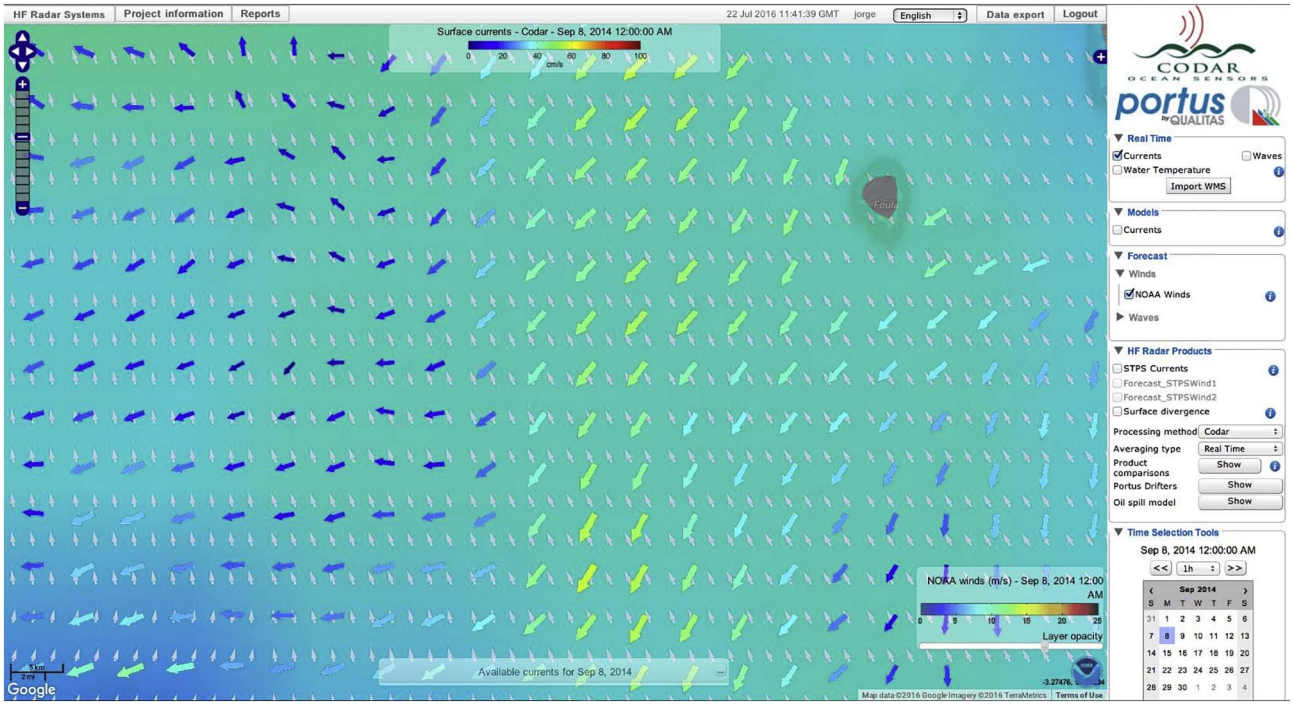

Fig. 5. Example of HF radar surface currents maps and GFS wind field close to the island of Foula in the Brahan area.

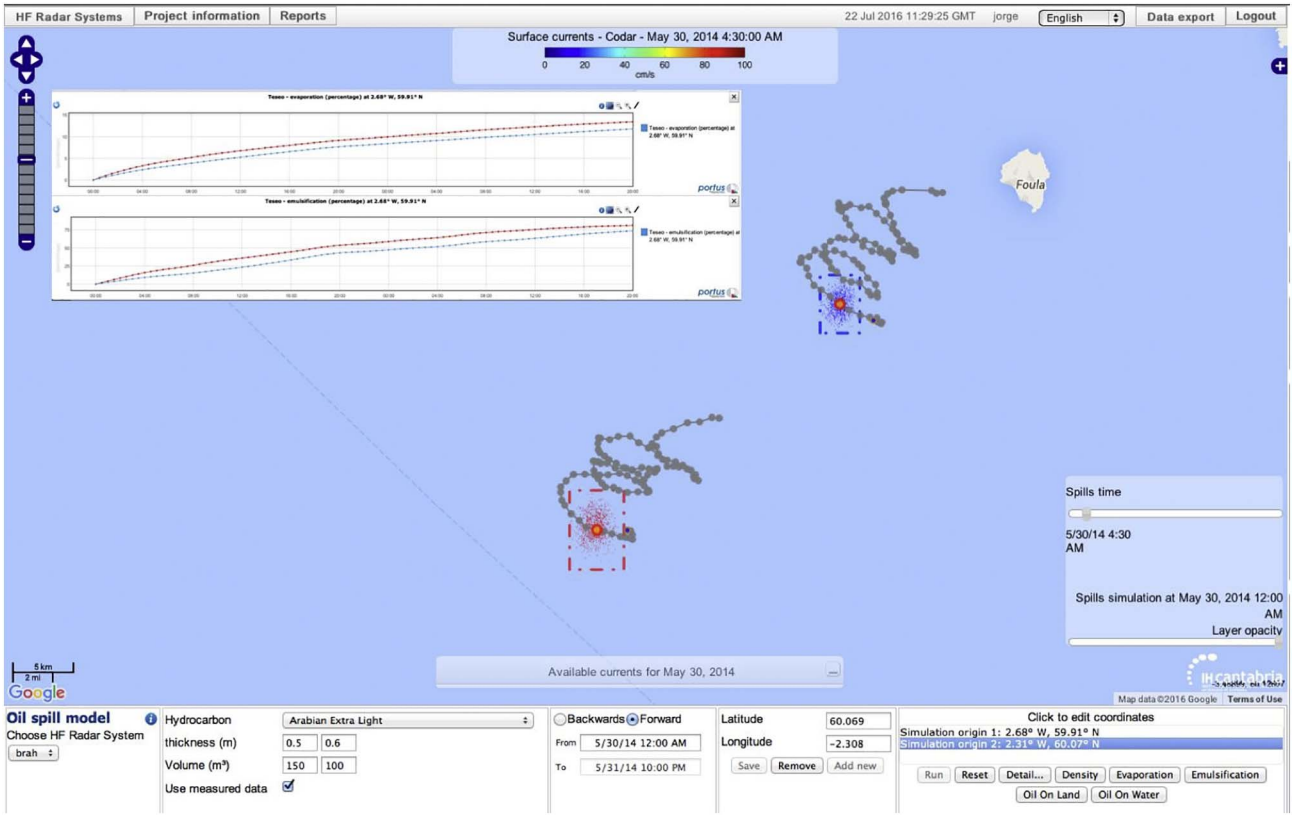

Fig. 6. Example of a hypothetical oil spill transport and fate simulation with two release points close to Foula in the Brahan area.

The oil spill trajectory simulations are run in a different remote server located at the IHCantabria data centre. This remote server automatically downloads forcing data for the transport model (GFS winds, OMA and STPS surface currents) and communicates with the management/information system through a web service. Figs. 5 and 6 show examples of the web-based user interface.

4. System validation

4.1. Drifter data

Drifter trajectory data were collected during two exercises carried out in October and December 2013 as part of the Brahan Project. A total

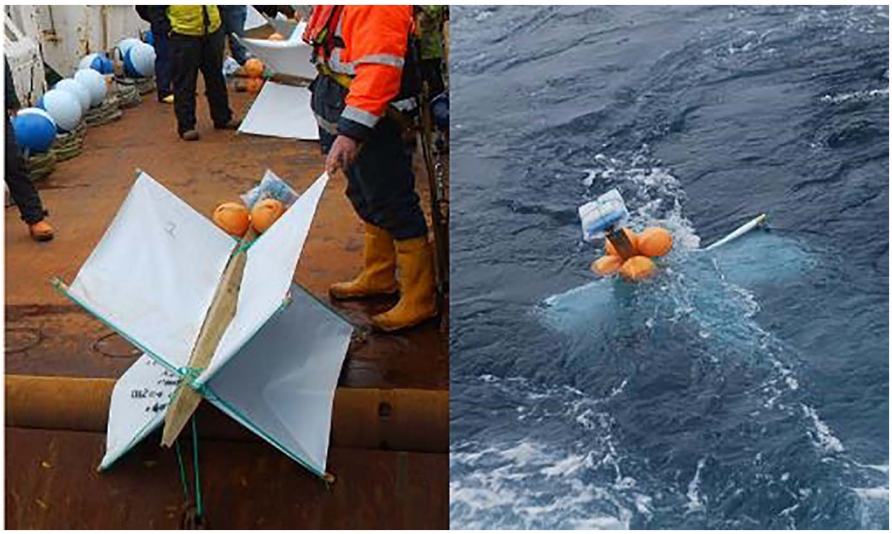

Fig. 7. Photographs of drifters used in the trajectory data collection.

of 18 drifters were deployed, ten during the first exercise and eight during the second.

The design of the drifters was based on the work of Davis (1985). The drifters were designed to be advected by surface currents with minimal influence of wind and surface waves (Fig. 7). Initial analysis of the behaviour of these drifters by MSS (Berx et al., 2014) suggests the drifter overestimates along-drift speed by approx. 6% (or 2 cm s^{-1} slippage at a mean drift rate of 34 cm s^{-1}), on average.

Drifters transmitted their positions via satellite in real time with an hourly time step. Until reaching the coast or stopping transmission, they generally followed long trajectories through the West Shetland Shelf, although in some cases just a relative small portion of the trajectories were within our study area, as shown in Fig. 8. Several gaps exist in their trajectory records due to transmission breakdowns during the drift. For these reasons, pre-processing of the drifter trajectory data was required. Taking into account the typical forecast horizon in an emergency oil spill response, 48-hour sections that remained wholly inside the HF radar domain were selected to be used as independent trajectories in the study (see Table 1).

4.2. Trajectory analysis

4.2.1. Simulations set-up

The trajectory forecasting capability of the system was validated by comparing the simulations against the entire set of drifter trajectories. The objective of the validation was twofold: firstly to analyze the accuracy of the simulations carried out with gap-free OMA currents and STPS predicted fields and, secondly, to assess the performance of HF radar derived data in comparison with HDM currents, typically used in oil spill operational systems. For this reason, four simulation tests were carried out: Test 1 – hindcast trajectories computed using OMA currents; Test 2 – forecast trajectories computed using STPS currents; Test 3 – forecast trajectories computed using HDM currents provided by an operational ocean forecasting system, and; Test 4 – forecast trajectories computed using Persistence fields. Persistence simply consists of continuing the latest nowcast condition into the future (in this case the OMA field at simulation time = 0), as a constant term. Note that for an operational application, OMA data (based on measured data) may be of value for backtracking purposes, while STPS (forecast) and HDM (forecast) currents may be of value for the prediction of oil spill trajectories.

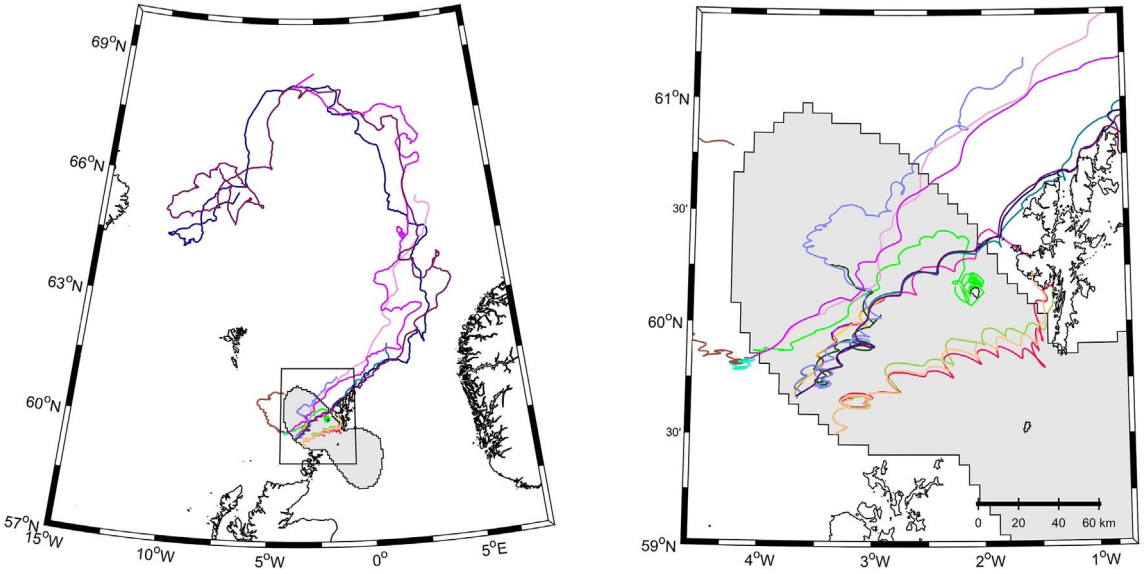

Fig. 8. Trajectory data collected during the drifter exercises. Left panel shows the complete trajectories and right panel shows the detail over the radar coverage area (grey filled sector).

Table 1
48-h independent sections extracted from the original drifter paths.

Exercise	Section ID	Initial time	Initial position (°E, °N)	Final time	Last position (°E, °N)
1	1	10/03 22:00	− 3.9855, 59.8593	10/05 22:00	− 3.5988, 59.9360
	2	10/05 22:00	− 3.5988, 59.9360	10/07 22:00	− 2.7231, 60.3255
	3	10/14 23:00	− 3.3935, 59.7598	10/16 23:00	− 3.2948, 59.8758
	4	10/14 23:00	− 3.3782, 59.7629	10/16 23:00	− 3.3344, 59.8405
	5	10/16 23:00	− 3.2948, 59.8758	10/18 23:00	− 2.9552, 60.0172
	6	10/16 23:00	− 3.3344, 59.8405	10/18 23:00	− 2.9296, 60.0215
	7	10/18 23:00	− 2.9296, 60.0215	10/20 23:00	− 3.5473, 60.3441
	8	10/20 23:00	− 3.5473, 60.3441	10/22 23:00	− 3.4114, 60.4448
	9	10/22 23:00	− 3.4114, 60.4448	10/24 23:00	− 2.9071, 60.4979
	10	10/24 23:00	− 2.9071, 60.4979	10/26 23:00	− 2.7316, 60.6423
2	1	12/11 3:00	− 3.6435, 59.6798	12/13 3:00	− 3.1467, 59.9495
	2	12/11 3:00	− 3.6448, 59.6792	12/13 3:00	− 3.1487, 59.9473
	3	12/13 3:00	− 3.1467, 59.9495	12/15 3:00	− 2.0302, 60.3309
	4	12/13 3:00	− 3.1482, 60.2144	12/15 2:00	− 2.4896, 60.6181
	5	12/13 3:00	− 3.2541, 59.6384	12/15 3:00	− 2.5167, 59.7740
	6	12/13 3:00	− 3.2619, 59.6321	12/15 3:00	− 2.5140, 59.7908
	7	12/11 4:00	− 3.9239, 59.8774	12/13 4:00	− 2.9485, 60.2916
	8	12/11 4:00	− 3.9363, 59.8716	12/13 3:00	− 3.1482, 60.2144
	9	12/12 7:00	− 3.1412, 59.8960	12/14 7:00	− 2.5751, 60.2294
	10	12/15 4:00	− 2.5055, 59.7808	12/17 4:00	− 1.6606, 59.8649
	11	12/15 4:00	− 2.5037, 59.7992	12/17 4:00	− 1.6710, 59.9279
	12	12/17 4:00	− 1.6606, 59.8649	12/19 4:00	− 1.5451, 60.0521

HDM currents in the study area were obtained from the Forecasting Ocean Assimilation Model 7 km Atlantic Margin model (FOAM AMM7) developed by the UK Met Office (O'Dea et al., 2012), which provides surface currents with 1 h temporal resolution and 7 km spatial resolution. These data correspond to the predicted currents provided by the operational forecasting system during the drifter exercises.

Taking into account the low-profile drifter design, aimed at minimizing wind effect, and the previous calibration of the system that shows that the wind drag coefficient (C_D) is close to 0 (Cardenas et al., 2015), the drifter trajectories were simulated forced only with currents. This procedure is widely used in drifter trajectory simulations (e.g., Liu et al., 2011a, b; Abascal et al., 2015). For each test, simulations were performed for the entire set of drifter trajectories (see Table 1), which represents a total of 22 independent trajectories. The forecast horizon was 48 h for Test 1 and Test 3 (OMA and numerical currents) and 12 h for Tests 2 and 4 (STPS and Persistence fields). A total of 1000 independent numerical particles were used in every simulation, the diffusive coefficient was set to D = 50 $m^2 s^{-1}$ (ASCE Task Committee, 1996) and a 60 s time step was used to calculate the time evolution of the particle positions.

4.2.2. Results

In this section, the differences between the simulations and the actual drifter trajectories are analyzed. For each test, actual and simulated trajectories were compared for all the 22 selected periods. For clarity, only a subset of the simulations is presented here. The results have been selected to show trajectories that are well simulated using both numerical and radar derived OMA currents and to show trajectories that are clearly improved using OMA currents. Nonetheless, note that these results are representative of the entire set of simulated trajectories.

In Figs. 9, 10, 11 and 12 the comparisons between actual and simulated trajectories for sections 2, 8 (Exercise 1) and 7, 10 (Exercise 2) are presented. Upper left panels show the simulation carried out with OMA currents (Test 1), upper right panels the simulation carried out with STPS predicted currents (Test 2), lower left panels show the simulations carried out with predicted numerical currents (Test 3) and lower right panels the simulation carried out with Persistence currents (Test 4). In each panel, the triangles represent the observed buoy positions, the point cloud represents the simulated particle positions and the circles represent the center of mass of the simulation (coinciding with the time of the buoy positions). Note that the simulation period for Test 2 and Test 4 is shorter (12 h) than for Tests 1 and 3 (48 h).

As it can be observed, simulations with OMA currents (Test 1) are in good agreement with the observed trajectories. In all cases, the accuracy of the simulations improves when OMA currents are used to compute the drifter trajectory. It is also worth noting the high quality of the simulations in this region carried out using the selected HDM currents (Test 3). However, even when HDM currents present a high skill to reproduce the drifter trajectories in this area, results are improved using OMA currents (see Fig. 11). Note that the improvement is more significant when the drifter follows a complex pattern, as the paths followed during section 8 of Exercise 1 (Fig. 10) and section 10 of Exercise 2 (Fig. 12). Regarding the simulations using STPS fields (Test 3), the difference between actual and numerical trajectories increases compared to the use of OMA currents. This behaviour is expected due to the fact that STPS currents are predictive fields whereas OMA currents are hindcast fields. However, a reasonable agreement between actual and STPS trajectories is observed during the first hours of the simulation, while more discrepancies are observed towards the final section. Simulations using Persistence fields (Test 4) always show a linear pattern, as should be expected. For this reason, these simulations behave reasonably well compared to actual drifter trajectories when drifter movement presents a simple pattern (Figs. 9 and 11) and major discrepancies are observed for complex drifter trajectories (Figs. 10 and 12). For nearly 80% of the simulated sections (17 out of 22), the STPS trajectories were closer to the actual drifter trajectories than those using Persistence fields.

In order to quantify the error, the model accuracy was measured by computing the distance (d) between the observed and the center of mass of the simulated trajectories. The distance was computed for every hour of the total trajectory section and averaged over all the simulations performed, according to the following equation.

$$d_m(t) = \frac{1}{N}\sum_{i=1}^{N}\sqrt{d_i^2} \tag{4}$$

where d_m is the average hourly separation distance, t is the time and N is the number of simulated sections (N = 22).

Fig. 13 shows the mean temporal evolution and standard deviation of the separation distance as a function of prediction time for Test 1 (upper left panel), Test 2 (upper right panel), Test 3 (lower left) and Test 4 (lower right). In Table 2 a summary of the distance error (d_m) for different time horizons of 3, 6, 9, 12, 24 and 48 h is presented.

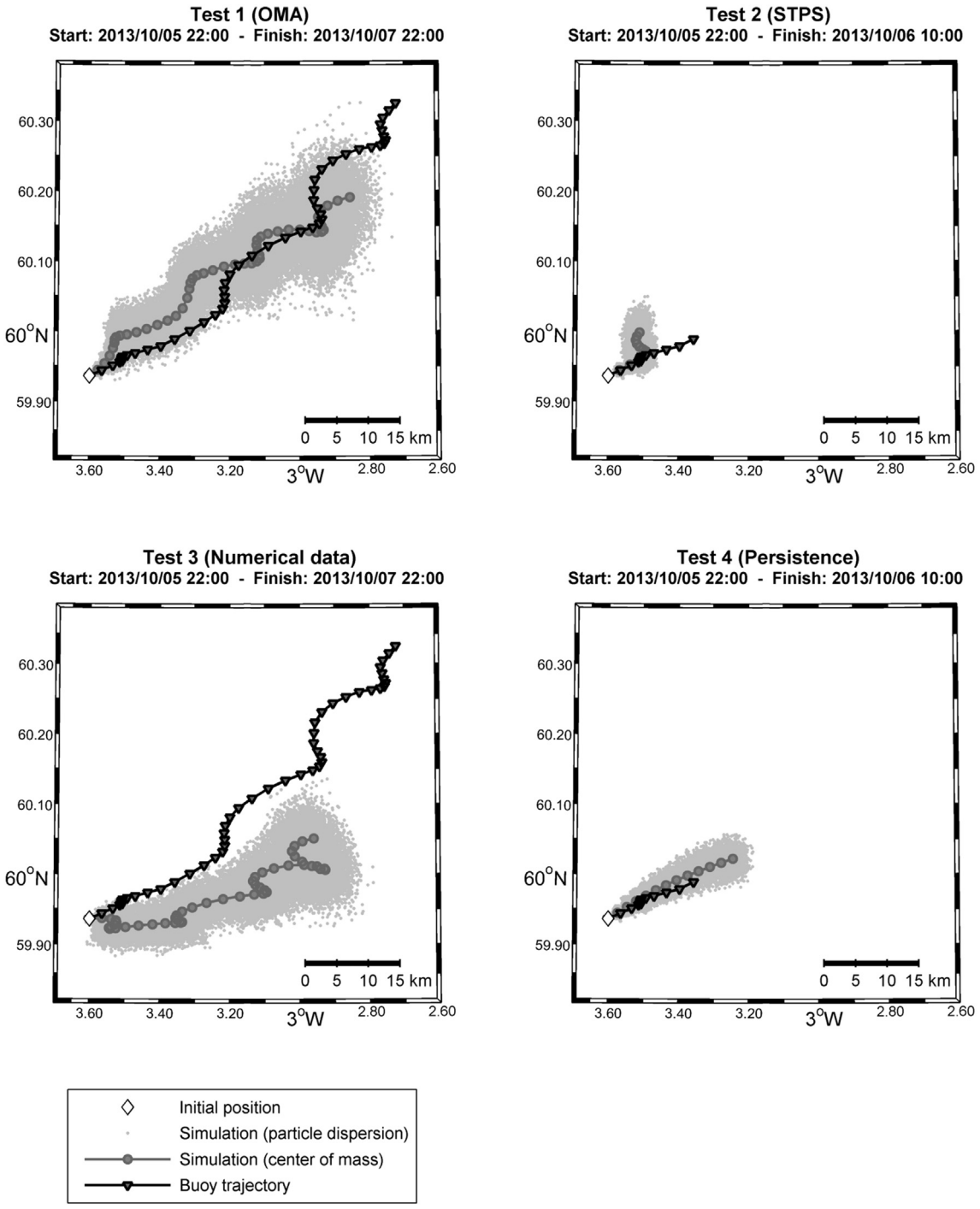

Fig. 9. Comparison between actual drifter trajectories (triangles) and simulated (circles) trajectories for section 2 of the Exercise 1 for all four tests.

In the four cases, the distance between actual and simulated trajectories increases over time. The mean separation is in general smaller when OMA currents fields are used to compute the trajectory of the buoys. However, it is worth noting the high skill of the HDM currents used to simulate the drifter trajectories in this region. The predicted trajectories with OMA and HDM currents produce nearly equivalent separation distances during the first hours of the simulation, with a mean separation distance (d_m) of 4 km at 9 h. From this time to the end of the simulation the error progressively increases using HDM currents. After 48 h, the distance between the real and simulated positions is 11 km using OMA currents and 18 km using HDM currents. These results show that using HF radar derived OMA currents reduces the error in the simulated trajectory, on average, by approximately 40% when compared to simulations using HDM currents.

Simulations carried out with STPS currents (Test 2) show a satisfactory agreement with actual drifter trajectories during the first hours of the simulation. A mean separation distance of 4.4 km is obtained after 6 h of simulation and 7.5 km after 12 h, which represents an improvement of, respectively, 36% and 29% compared to simulations using Persistence. However, the analysis shows that simulations using HDM currents yield better results than those using STPS currents. The mean separation distance using HDM currents is reduced by approximately 21% after 12 h of simulation compared to the results using STPS currents. These differences can be related to several factors, including sudden wind variability during the October and December 2013 drifter releases, which is not included properly within this STPS

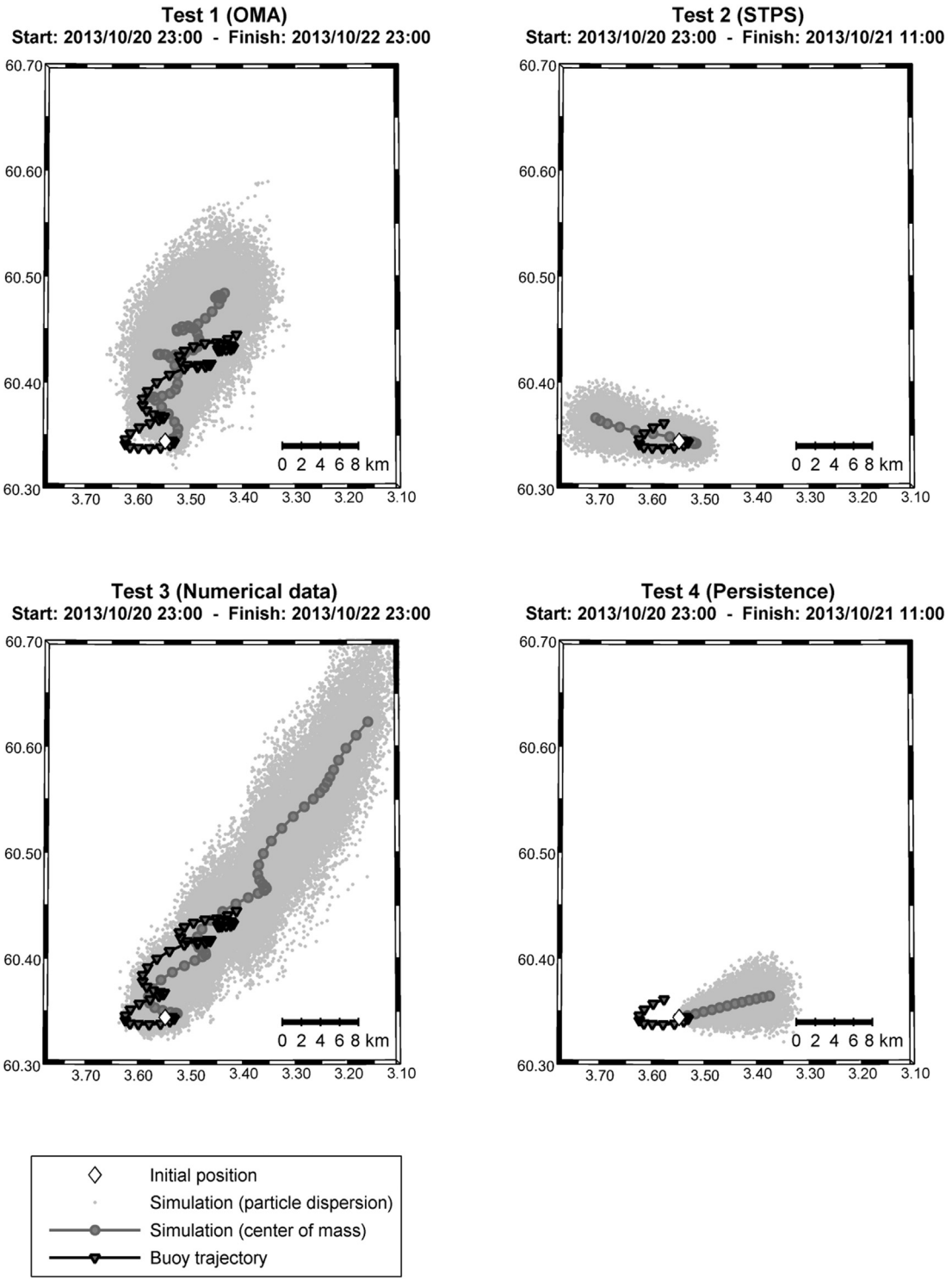

Fig. 10. Comparison between actual drifter trajectories (triangles) and simulated (circles) trajectories for section 8 of the Exercise 1 for all four tests.

approach.

These results show a very good forecast skill for the FOAM AMM (HDM) model up to 12 h and a satisfactory skill of the STPS field to forecast the trajectory for the first hours (up to 6 h) of the simulation, thus showing the potential of this technique as a forecast tool for short term trajectory simulations in areas where complex high quality HDMs are not available.

5. Conclusions

A novel operational oil spill modelling system based on HF radar currents has been successfully developed and tested in a northwest European shelf sea. The innovative approach consists of the use of gap-free HF radar surface currents based on Open Modal Analysis and Short Term Predicted currents to operationally provide forward and backward predictions of oil spills. Our HF radar-based system has been demonstrated to be potentially highly useful and innovative in oil spill response, both to provide support in an oil spill emergency (forecasting)

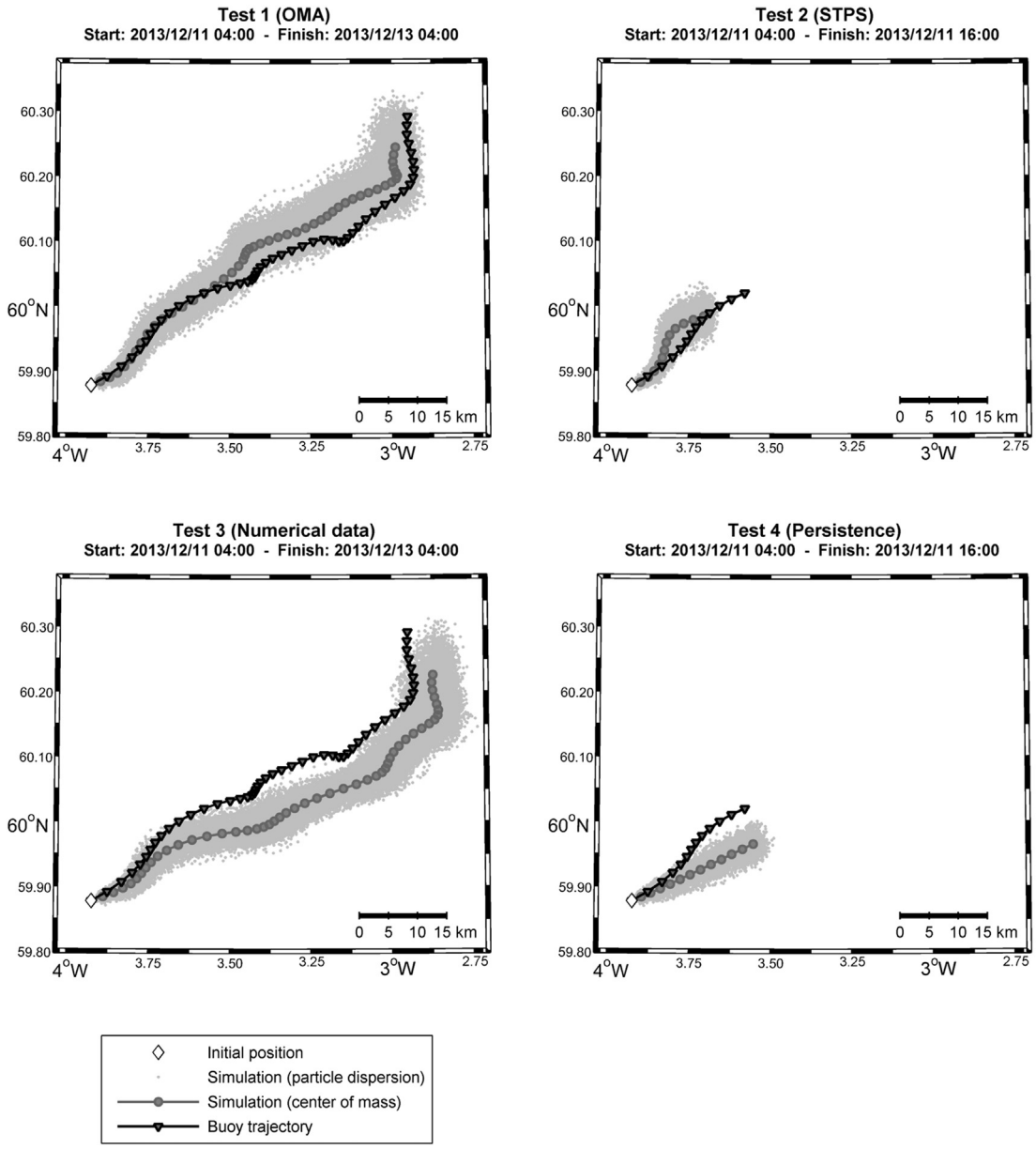

Fig. 11. Comparison between actual drifter trajectories (triangles) and simulated (circles) trajectories for section 7 of the Exercise 2 for all four tests.

as well as to identify illegal discharges and potential polluters (back-tracking). This system was working operationally during the period June 2014–August 2014.

The oil spill trajectory forecasting system was extensively validated by means of a set of 18 drifting buoys deployed during two drift experiments carried out in the study area. A sensitivity analysis was carried out to assess the accuracy of OMA and STPS for oil spill simulations and to evaluate the benefits of HF radar data in relation to the use of HDM currents.

Comparisons between actual (drifter) and simulated trajectories showed that, in general, the simulations integrating OMA gap-free velocity fields were more accurate than those performed with HDM currents. It is worth noting that, given the high-quality of the HDM currents, there is not an improvement using OMA currents during the first 9 h of the simulation. However, a progressive increase in the error using HDM currents was observed after this time. After 48 h the distance between the real and simulated positions was found to be 11 km using OMA currents and 18 km using HDM currents. These results demonstrated that using OMA currents the error in the simulated trajectory was reduced, on average, by approximately 40%. Taking into account that OMA currents are based on observations, this analysis also suggests that there may be benefits using HF radar currents to improve backtracking modes in operational oil spill modelling systems.

The forecast skill of the STPS method was found appropriate up to 6 h. At that time, the mean separation distance between actual and numerical positions using STPS currents was found to be 36% shorter than using Persistence and ~26% larger than those performed with OMA currents. These results showed a satisfactory trajectory forecast skill using the STPS technique to compute the drifter trajectories. However, the difference between STPS and OMA trajectory simulations increased to 40% at the end of the simulation period (12 h), indicating the limitations of the STPS technique for longer forecast periods. According to previous studies (Liu et al., 2011a, b), this result also shows the importance of frequent re-initialization in operational oil spill trajectory modelling.

The operational forecast system presented in this paper represents an improvement in the capacity to respond to oil spill pollution. The analysis performed suggests the potential benefits of using HF radar derived currents in operational oil spill modelling systems. On the one hand, HF radar currents may be used to improve the accuracy of

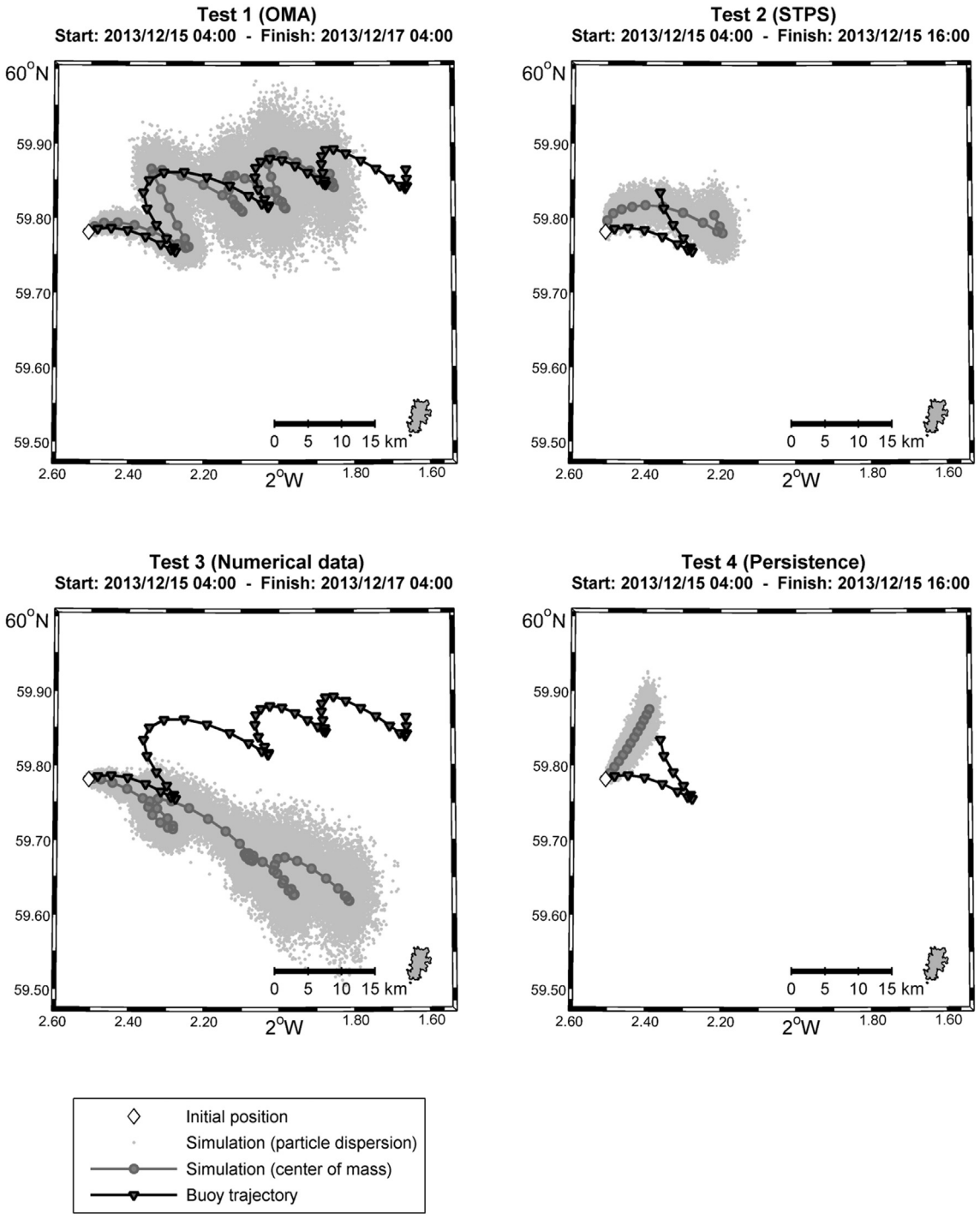

Fig. 12. Comparison between actual drifter trajectories (triangles) and simulated (circles) trajectories for section 10 of the Exercise 2 for all four tests.

simulations for backtracking purposes. On the other hand, these data can also be used to provide a forecast tool for short term trajectory simulations in areas where complex high quality HDMs are not available. Further work is required to improve the accuracy for short-term forecasts in this area by including surface wind stress forecast into the STPS model. Future work should also include assessing the skill of trajectory simulations using original HF radar currents in areas without gaps and comparing results with the ones that have been obtained in this study using OMA gap-free current fields and HDM currents.

Acknowledgements

This work was partially funded from a grant from Iceland, Liechtenstein and Norway through the EEA Grants under the research project IDI-20140011 (NEMOT4OGI) and by the Spanish Ministry of Economy and Competitiveness (MINECO) under the research projects TRA2011-28900 (PLVMA) and TRA2014-59570-R (PLVMA3D). MC would like to thank the Spanish Ministry of Economy and Competitiveness (MINECO) for the funding under the FPI Program. We would also like to thank all partners of the Brahan Project for their help and support and Jan Maksymczuk from the UK Met Office for kindly providing the data from the FOAM-AMM model.

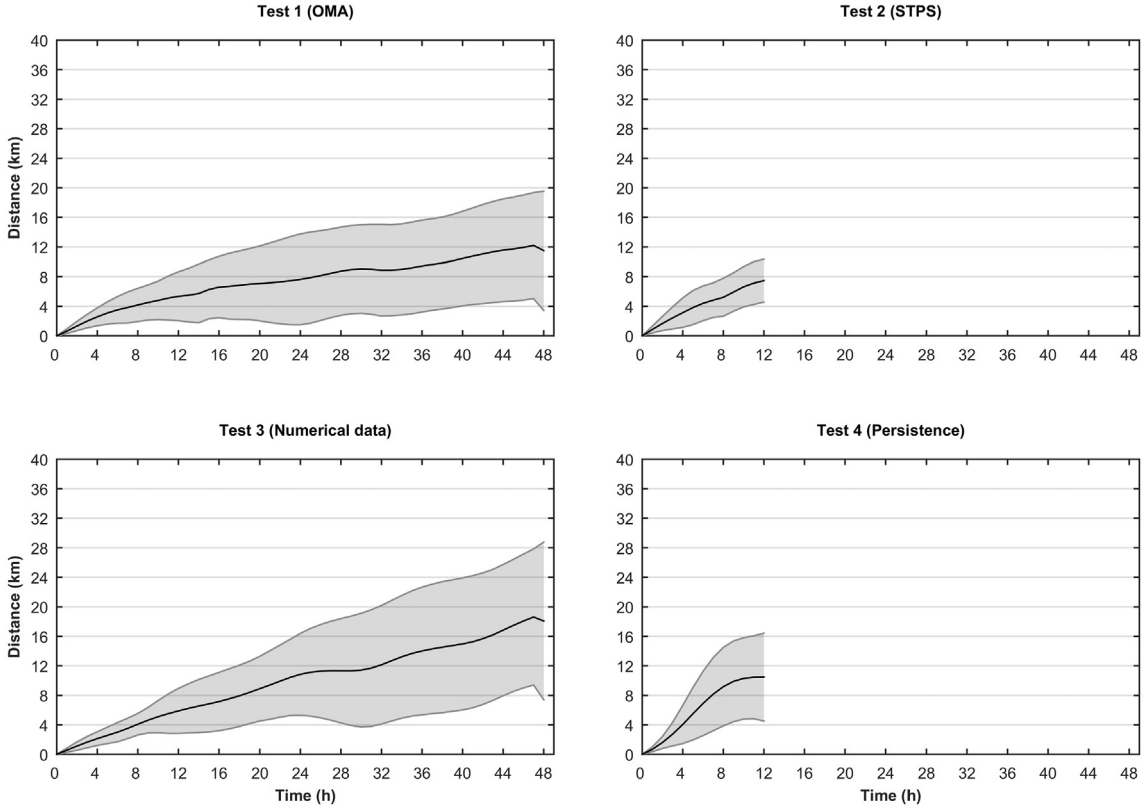

Fig. 13. Evolution of the separation distance between actual drifter and simulated trajectories for Test 1 (upper left), Test 2 (upper right), Test 3 (lower left) and Test 4 (lower right).

Table 2
Summary of the separation distance between the observed and simulated trajectories for all four tests.

Error	Test	+ 3 h	+ 6 h	+ 9 h	+ 12 h	+ 24 h	+ 48 h
d_m (*Km*)	1	1.99 ± 0.91	3.52 ± 1.80	4.19 ± 2.37	5.35 ± 3.30	7.63 ± 6.13	11.15 ± 8.05
	2	2.44 ± 1.49	4.41 ± 2.35	5.22 ± 2.59	7.46 ± 2.88	–	–
	3	1.66 ± 0.77	3.01 ± 1.30	4.09 ± 1.73	5.89 ± 3.05	10.85 ± 5.55	18.08 ± 10.67
	4	2.75 ± 1.60	6.90 ± 4.35	9.90 ± 5.47	10.48 ± 5.95	–	–

References

Abascal, A.J., Castanedo, S., Gutierrez, A.D., Comerma, E., Medina, R., Losada, I.J., 2007. TESEO, an operational system for simulating oil spills trajectories and fate processes. In: Proceedings, ISOPE-2007: The 17th International Offshore Ocean and Polar Engineering Conference. Lisbon, Portugal. 3. pp. 1751–1758.

Abascal, A.J., Castanedo, S., Medina, R., Losada, I.J., Alvarez-Fanjul, E., 2009. Application of HF radar currents to oil spill modelling. Mar. Pollut. Bull. 58 (2), 238–248.

Abascal, A.J., Castanedo, S., Fernández, V., Medina, R., 2012. Backtracking drifting objects using surface currents from high-frequency (HF) radar technology. Ocean Dyn. 62, 1073–1089.

Abascal, A.J., Castanedo, S., Minguez, R., Medina, R., Liu, Y., Weisberg, R.H., 2015. Stochastic Lagrangian trajectory modeling of surface drifters deployed during the Deepwater Horizon oil spill. In: Proc. 38th AMOP Tech. Seminar Env. Contamination & Response, Env. & Climate Change Canada, Ottawa, ON, pp. 71–99.

Ambjörn, C., 2008. Seatrack Web forecasts and backtracking of oil spills - an efficient tool to find illegal spills using AIS. In: US/EU-Baltic International Symposium. IEEE/OES.

ASCE Task Committee, 1996. State-of-the-art review of modeling transport and fate of oil spills. J. Hydraul. Eng. 122 (11), 594–609.

Barrick, D.E., Evans, M.W., Weber, B.L., 1977. Ocean surface currents mapped by radar. Science 198, 138–144.

Barrick, D., Fernández, V., Ferrer, M.I., Whelan, C., Breivik, Ø., 2012. A short-term predictive system for surface currents from a rapidly deployed coastal HF radar network. Ocean Dyn. 62 (5), 725–740.

Beaugrand, G., 2004. The North Sea regime shift: evidence, causes, mechanisms and consequences. Prog. Oceanogr. 60 (2–4), 245–262.

Berx, B., Dunn, J., Geldart, M., Hughes, S., Lee, D., 2014. MSS Davis CODE drifter. Marine Scotland Science report. (Retrieved June, 2016 from:). http://www.gov.scot/Resource/0046/00461208.pdf.

Breivik, Ø., Sætra, Ø., 2001. Real-time assimilation of HF radar currents into a coastal ocean model. J. Mar. Syst. 28 (161), 182.

Breivik, O., Allen, A., Maisondieu, C., Olagnon, M., 2013. Advances in search and rescue at sea. Ocean Dyn. 68, 83–88.

Cardenas, M., Abascal, A.J., Castanedo, S., Chiri, H., Ferrer, M.I., Sanchez, J., Medina, R., Turrell, W.R., Hughes, S., Gallego, A., Berx, B., 2015. Spill trajectory modelling based on HR radar currents in the North Sea: validation with drifter buoys. In: Proceedings, The Thirty-Eighth AMOP Technical Seminar, Environmental Canada, Ottawa, ON, pp. 124–142.

Castanedo, S., Medina, R., Losada, I.J., Vidal, C., Méndez, F.J., Osorio, A., Juanes, J.A., Puente, A., 2006. The Prestige oil spill in Cantabria (Bay of Biscay). Part I: operational forecasting system for quick response, risk assessment, and protection of natural resources. J. Coast. Res. 1474–1489.

Castanedo, S., Perez-Diaz, B., Abascal, A.J., Cardenas, M., Olabarrieta, M., Medina, R., Receveur, J., Evrard, E., Guyomarch, J., 2014. A high resolution operational oil spill model at santander bay (Spain): implementation and validation. In: Proceedings International Oil Spill Conference 2014. American Petroleum Institute, pp. 516–530.

Christiansen, B.M., 2003. 3D Oil Drift and Fate Forecast at DMI. Technical Report No. 03-36. Danish eteorological Institute, Denmark.

Davis, R.E., 1985. Drifter observations of coastal surface currents during CODE: the method and descriptive view. J. Geophys. Res. 90 (C3), 4741–4755.

Dean, R.G., Dalrymple, R.A., 1991. Water Wave Mechanics for Engineers and Scientists. Advanced Series on Ocean Engineering. 2 World Scientific, Singapore.

Edwards, K.P., Werner, F.E., Blanton, B.O., 2006. Comparison of observed and modeled drifter trajectories in coastal regions: an improvement through adjustments for observed drifter slip and errors in wind fields. J. Atmos. Ocean. Technol. 23 (11), 1614–1620.

Environmental Modeling Center, 2003. The GFS atmospheric model. NOAA/NCEP/Environmental Modeling Center Office note 442. (14 pp. Retrieved June, 2016 from). http://www.emc.ncep.noaa.gov/officenotes/FullTOC.html.

Fay, J.A., 1971. Physical processes in the spread of oil on a water surface. In: Proceedings International Oil Spill Conference 1971. American Petroleum Institute, pp. 4e63–4467.

Frolov, S., Paduan, J., Cook, M., Bellingham, J., 2011. Improved statistical prediction of surface currents based on historic HF-Radar observations. Ocean Dyn, SAR2011.

Graber, H.C., Haus, B.K., Shay, L.K., Chapman, R.D., 1997. HF radar comparisons with moored estimates of current speed and direction: expected differences and implications. J. Geophys. Res. 102, 18,749–18,766.
Harlan, J., Terrill, E., Hazard, L., Keen, C., Barrick, D.E., Whelan, C., Howden, S., Kohut, J., 2010. The integrated ocean observing system high frequency radar network: status and local, regional and national applications. Mar. Soc. Pap. J. 122e–1125.
Hoteit, I., Cornuelle, B., Kim, S.Y., Forget, G., Kohl, A., Terrill, E., 2009. Assessing 4D-VAR for dynamical mapping of coastal high-frequency radar in San Diego. Dyn. Atmos. Oceans 48, 175–197.
Hubbard, M., Barrick, D., Garfield, N., Pettigrew, J., Ohlmann, C., Gough, M., 2013. A new method for estimating high-frequency radar error using data from Central San Francisco Bay. Ocean Sci. J. 1–12.
Hunter, J.R., Craig, P.D., Phillips, H.E., 1993. On the use of random walk models with spatially variable diffusivity. J. Comput. Phys. 106 (2), 366–376.
Huthnance, J.M., 1997. North Sea interaction with the North Atlantic ocean. In: Deutsche Hydrographische Zeitschrift. 49. pp. 153–162.
Kaplan, D.M., Largier, J., Botsford, L.W., 2005. HF radar observations of surface circulation off Bodega Bay (Northern California, USA). J. Geophys. Res. 110, C10020.
Kaplan, D.M., Leiken, F., 2007. Spatial interpolation and filtering of surface current data based on open boundary modal analysis. J. Geophys. Res. 112, C12007 (20 pp).
Lekien, F., Coulliette, C., 2004. Open-boundary modal analysis: interpretation, extrapolation, and filtering. J. Geophys. Res. 109 (C12004) (13 pp).
Lekien, F., Gildor, H., 2009. Computation and approximation of the length scales of harmonic modes with application to the mapping of surface currents in the Gulf of Eilat. J. Geophys. Res. 114, C06024.
Lipa, B.J., Barrick, D.E., 1986. Extraction of sea state from HF radar sea echo: mathematical theory and modeling. Radio Sci. 21, 81–100.
Lipa, B., Barrick, D.E., Alonso-Martirena, A., Fernandes, M., Ferrer, M.I., Nyden, B., 2014. Brahan project high frequency Radar Ocean measurements: currents, winds, waves and their interactions. Remote Sens. 6 (12), 12094–12117.
Lipphardt, B.L., Kirwan, A.D., Grosch, C.E., Lewis, J.K., Paduan, J.D., 2000. Blending HF radar and model velocities in Monterey Bay through normal mode analysis. J. Geophys. Res. 105 (C2), 3425–3450.
Liu, Y., Weisberg, R.H., Hu, C., Zheng, L., 2011b. Tracking the deepwater horizon oil spill: a modeling perspective, EOS transactions. Am. Geophys. Union 92 (6), 45–46.
Liu, Y., MacFadyen, A., Ji, Z.-G., Weisberg, R.H., 2011a. Monitoring and Modeling the Deepwater Horizon Oil Spill: A Record-Breaking Enterprise, Geophysical Monograph Series. vol. 195 AGU/geopress, Washington D.C. (271 pp.).
Liu, Y., Weisberg, R.H., Hu, C., Zheng, L., 2011c. Trajectory forecast as a rapid response to the deepwater horizon oil spill, in monitoring and modeling the deepwater horizon oil spill: a record-breaking enterprise. In: Geophysical Monograph Series. 195. pp. 153–165. http://dx.doi.org/10.1029/2011GM001121.
Liu, Y., Weisberg, R.H., Merz, C.R., 2014. Assessment of CODAR and WERA HF radars in mapping currents on the West Florida shelf. J. Atmos. Ocean. Technol. 31, 1363–1382. http://dx.doi.org/10.1175/JTECH-D-13-00107.1.
Liu, Y., Kerkering, H., Weisberg, R.H., 2015. Coastal Ocean Observing Systems. (461 pp., ISBN 978-0-12-802022-7) Elsevier (Academiec Press), London, UK.
Long, R., Barrick, D., 2007. Surface Current Measurements During Safe Seas 2006: Comparison and Validation of Measurements From High-Frequency Radar and the Quick Release Estuarine Buoy, Proceedings of the MTS/IEEE OCEANS'07 Conference. Vancouver, BC, Canada.
Lorente, P., Soto-Navarro, J., Álvarez-Fanjul, E., Piedracoba, S., 2014. Accuracy assessment of high frequency radar current measurements in the Strait of Gibraltar. J. Oper. Oceanogr. 7 (2).
Mackay, D., Paterson, S., Trudel, K., 1980. A Mathematical Model of oil Spill Behaviour. Environmental Emergency Branch, Environmental Impact Control Directorate, Environmental Protection Service, Environment Canada.
Maier-Reimer, E., Sündermann, J., 1982. On tracer methods in computational hydrodynamics. In: Engineering Applications of Computational Hydraulics. 1. pp. 198–217.
O'Dea, E.J., Arnold, A.K., Edwards, K.P., Furner, R., Hyder, P., Martin, M.J., Siddorn, J.R., Storkey, D., While, J., Holt, J.T., Liu, H., 2012. An operational ocean forecast system incorporating NEMO and SST data assimilation for the tidally driven European North-West shelf. J. Oper. Oceanogr. 5 (1), 3–17. http://dx.doi.org/10.1080/1755876X.2012.11020128.
O'Donnell, J., Ullman, D., Spaulding, M., Howlett, E., Fake, T., Hall, P., Tatsu, I., Edwards, C., Anderson, E., McClay, T., Kohut, J., Allen, A., Lester, S., Lewandowski, M., 2005. Integration of Coastal Ocean Dynamics Application Radar (CODAR) and Short-Term Prediction System (STPS) Surface Current Estimates Into the Search and Rescue Optimal Planning System (SAROPS), U.S. Coast Guard Tech. Rep., DTCG39-00-D-R00008/HSCG32-04-J-100052 .
Oke, P.R., Allen, J.S., Miller, R.N., Egbert, G.D., Kosro, P.M., 2002. Assimilation of surface velocity data into a primitive equation coastal ocean model. J. Geophys. Res. 107 (C9), 3122. http://dx.doi.org/10.1029/2000JC000511.
Otto, L., Zimmerman, J.T.F., Furnes, G.K., Mork, M., Sætre, R., Becker, G., 1990. Review of the physical oceanography of the North Sea. Neth. J. Sea Res. 26 (2–4), 168–238.
Paduan, J., Shulman, I., 2004. HF radar data assimilation in the Monterey Bay area. J. Geophys. Res. 109 (CO7S09). http://dx.doi.org/10.1029/2003JC001949.
Price, J.M., Reed, M., Howard, M.K., Johnson, W.R., JI, Z., Marshall, C.F., Guinasso Jr., N.L., Rainey, G.B., 2006. Preliminary assessment of an oil-spill trajectory model using a satellite-tracked, oil-spill-simulating drifters. Environ. Model. Softw. 21, 258–270.
Roarty, H., Hazard, L., Fanjul, E.A., 2016. Growing network of radar systems monitors ocean surface currents. Eos 97http://dx.doi.org/10.1029/2016EO049243. (Published on 5 April 2016).
Rutledge, G.K., Alpert, J., Ebuisaki, W., 2006. NOMADS: a climate and weather model archive at the National Oceanic and Atmospheric Administration. Bull. Am. Meteorol. Soc. 87, 327–341.
Stewart, R.H., Joy, J.W., 1974. HF radio measurements of surface currents. Deep-Sea Res. 21, 1039–1049.
Stiver, W., Mackay, D., 1984. Evaporation rate of spills of hydrocarbons and petroleum mixtures. Environ. Sci. Technol. 18 (11), 834–840.
Svendsen, E., Sætre, R., Mork, M., 1991. Features of the northern North Sea circulation. Cont. Shelf Res. 11 (5), 493–508.
Turrell, W.R., 1992a. The east Shetland Atlantic inflow. ICES Mar. Sci. Symp. 195, 127–143.
Turrell, W.R., 1992b. New hypotheses concerning the circulation of the northern North Sea and its relation to North Sea fish stock recruitment. ICES J. Mar. Sci. 49, 107–123.
Turrell, W.R., Berx, B., Gallego, A., Hughes, S., O'Hara-Murray, R., Sanchez, J., Pereira, B., Alonso-Martirena, A., 2014. HF radar in NW Europe: The Brahan Project. In: Proceedings of the 7th EuroGOOS Conference, "Operational Oceanography for Sustainable Blue Growth", Lisbon, (28-30 October, 2014). 10.13140/RG.2.2.17080.34562.
Ullman, D., O'Donnell, J., Edwards, C., Fake, T., Morschauser, D., Sprague, M., Allen, A., Krenzien, B., 2003. Use of Coastal Ocean Dynamics Application Radar (CODAR) Technology in U. S. Coast Guard Search and Rescue Planning, U. S. Coast Guard Rep., CG-D-09-03. (40 pp).
Ullman, D.S., O'Donnell, J., Kohut, J., Fake, T., Allen, A., 2006. Trajectory prediction using HF radar surface currents: Monte Carlo simulations of prediction uncertainties. J. Geophys. Res. 111 (C12005), 1–14.
Zelenke, B.C., 2005. An Empirical Statistical Model Relating Winds and Ocean Surface Currents: Implications for Short-Term Current Forecasts. (M.Sc. Thesis) Oregon State University, Corvallis, OR.